*Volume 0 (), Number 0*

# A Connectivity-Aware Multi-level Finite-Element System for Solving Laplace-Beltrami Equations

Ming Chuang and Michael Kazhdan

Johns Hopkins University, Baltimore MD, USA



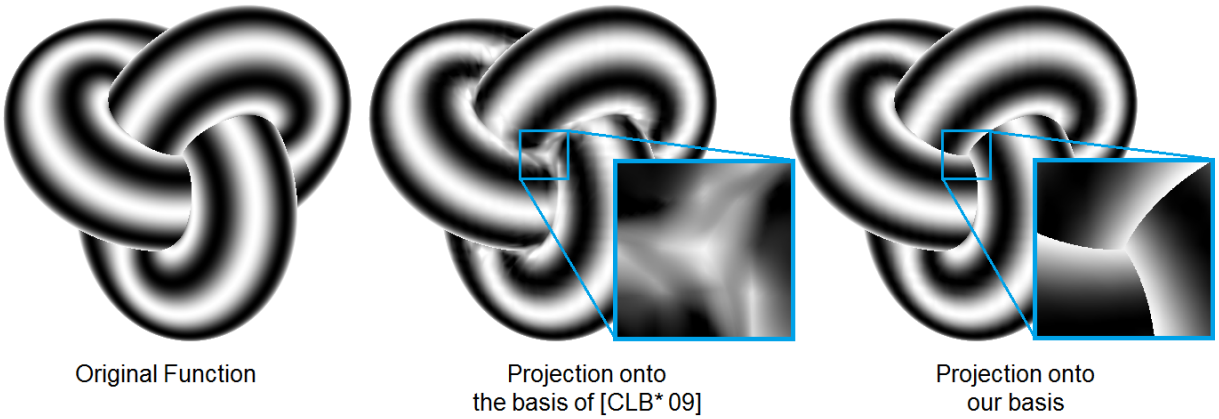


**Figure 1:** *A "knot" model with a stripe texture* (left) *projected onto Chuang* et al.*'s function space* (middle) *and our connectivity-aware function space* (right). *Due to the coupling of function values, Chuang* et al.*'s approach fails to reproduce the correct texture when points are close in Euclidean space but are geodesically distant. By designing our function space to be aware of local connectivity, we can fit the geodesically distant patches independently, resulting in a better reproduction of the original texture.*

**Abstract**

*Recent work on octree-based finite-element systems has developed a multigrid solver for Poisson equations on meshes. While the idea of defining a regularly indexed function space has been successfully used in a number of applications, it has also been noted that the richness of the function space is limited because the function values can be coupled across locally disconnected regions. In this work, we show how to enrich the function space by introducing functions that resolve the coupling while still preserving the nesting hierarchy that supports multigrid. A spectral analysis reveals the superior quality of the resulting Laplace-Beltrami operator and applications to surface flow demonstrate that our new solver more efficiently converges to the correct solution.*

Categories and Subject Descriptors (according to ACM CCS): I.3.3 [Computer Graphics]: Picture/Image Generation—Line and curve generation

## 1. Introduction

Solving the Poisson equation on meshes is essential in numerous geometry-processing applications. The task is most often formulated in terms of finite elements and two challenges commonly arise: discretizing the space of functions on meshes and solving the resulting system of equations.

For discretizing the system, the most ubiquitous approach is to use tent-functions centered at mesh vertices [Dzi88], resulting in the classical cotangent-weight formula for triangle meshes [PP93]. For solving the sytem, black-box solvers like Algebraic Multigrid [RS87, HY00] (iterative) and CHOLMOD [DH99, Dav11] (direct) have been popular.

Recently, Chuang *et al.* proposed an alternate framework that addresses both aspects simultaneously [CLB*09]. The idea is to define a function space in 3D and then restrict the 3D functions to the mesh. There are several advantages in doing so: (1) the independence of the function space from the mesh helps define a Laplace-Baltrami operator that does not depend on the tessellation; (2) the nesting structure of the function space supports an efficient multigrid solver; and (3) the regularity of the function space can be leveraged in parallelizaing the solver.

Though the approach has been successfully applied in a number of applications [CK11a, CK11b], it has been noted to produce artifacts because Euclidean distances are used to infer geodesic proximity. In particular, function values on locally disconnected components tend to be coupled when they are close in 3D, diminishing the richness of the function space (Figure 1). This also reduces the effectiveness of the multigrid solver, as disconnected regions are more likely to support the same basis function at coarser resolutions.

The goal of this work is to address this coupling issue without sacrificing the regularity and nesting structure of the function space. The key idea is to make the function space *connectivity-aware*. The function space is enriched by splitting existing functions such that the support of each new function is connected.

The paper is organized as follows. After a brief literature survey in Section 2, we review Chuang *et al.*'s approach in Section 3, setting up a context that facilitates the presentation of our approach in Section 4. In section 5, we conduct a spectral analysis revealing the improved quality of our Laplace-Beltrami operator, we show the superior convergence of the resulting multigrid sovler, and we demonstrate the competitiveness of our solver with the state-of-the-art CHOLMOD solver [Dav11] in a surface flow application. Finally, we conclude by summarizing our work and discussing directions for future research in Section 6.

## 2. Related Work

Solving a Poisson-like system is a fundamental step in numerous geometry-processing applications, including mesh editing [SCOL*04], mesh deformation [SA07], surface reconstruction [KBH06], surface fairing [Tau95, DMSB99], geometry sharpening/smoothing [CK11b], and surface parameterization [FH05].

Defining the discrete Laplacian operator on meshes has attracted a great deal of research in the computer graphics community. Graph-based, combintorial operators have advantages of simplicity and efficiency [Tau95, Zha04]. Geometry-driven operators taking angles and areas into account give rise the ubiquitous cotangent Laplacian [PP93, Flo03]. Recently, an operator based on intrinsic Delaunay triangulation has been proposed that addresses the problem of non-convex weighting [FSBS06, BS07]. We refer the reader to [WMKG07] for a study of the tradeoffs between different operators.

Solving the resulting system of equations is also of essential importance. Poisson-like systems are usaully sparse and direct sparse solvers have been a popular choice when memory is not a concern [DH99, Dav04, Li05]. In particular, when the system is symmetric and positive-definite, Cholesky factorization is often favored due to its numerical stability and efficiency [GVL96]. Furthermore, when the system is fixed but needs to be solved repeatedly for a constraint that varies over the course of an application, the factorization cost can be amortized, making these sparse factorization techniques an appealing option [SCOL*04].

Multigrid methods have also been used [BHM00]. Their low memory usage and ability to dampen low-frequency errors efficiently make them preferable to direct solvers when the problem size is exceedingly large and/or the exact solution is not necessary. To define the hierarchical structure on unstructured domains, "black-box" algebraic multigrid methods [RS87] that rely solely on algebraic information encoded in matrices have been studied [CFH*00, BCF*01, CFH*03]. Additionally, more geometry-driven approaches that rely on the design of mesh hierarchies have appeared in different contexts of geometry-procesing [KCVS98, CDR00, SK01, RL03, AKS05, SYBF06, SBZ09].

## 3. Review

In this section, we briefly review the FEM formulation for solving the Poisson equations on meshes and Chuang *et al.*'s choice of function spaces [CLB*09, CK11a, CK11b].

### 3.1. Finite Elements on Meshes

Given a Riemannian 2-manifold $\mathcal{M}$ and a continuous function $f : \mathcal{M} \to \mathbb{R}$, solving the Poisson equations amounts to finding another function $u$ on $\mathcal{M}$ whose Laplacian is $f$, i.e.,

$$\Delta_{\mathcal{M}} u = f \tag{1}$$

with $\Delta_{\mathcal{M}}$ denoting the Laplace-Beltrami operator, the generalization of the Laplace operator to $\mathcal{M}$.

Instead of looking for the exact solution within the infinite-dimensional space of functions on $\mathcal{M}$, a finite-elements system seeks an approximate solution within a finite-dimensional subspace $\mathcal{B} : \mathcal{M} \to \mathbb{R}$ spanned by the functions $\{b_1(p), \cdots, b_n(p)\}$. This is done by projecting both sides of Equation 1 onto $\mathcal{B}$ and solving an $n \times n$ lin-

ear system $L\mathbf{u} = \mathbf{f}$ where

$$L_{i,j} = \int_{\mathcal{M}} \Delta b_i(p) \cdot b_j(p) dp = -\int_{\mathcal{M}} \langle \nabla b_i(p), \nabla b_j(p) \rangle dp$$
$$\mathbf{f}_i = \int_{\mathcal{M}} f(p) \cdot b_i(p) dp \tag{2}$$

The second equality in the first line uses the *weak formulation* derived from Stokes' Theorem. It is correct when $\mathcal{M}$ is closed or when either the test functions or the normal derivatives vanish at the boundary. The best solution within $\mathcal{B}$ is then $u(p) = \sum_{i=1}^{n} \mathbf{u}_i b_i(p)$.

### 3.2. 3D B-Splines on Meshes

To set up $\mathcal{B}$, Chuang *et al.* start from a space of functions on $\mathbb{R}^3$ (independent of $\mathcal{M}$) that are piecewise trilinear within a *regular* voxel grid $\mathcal{G}^N$ of resolution $N \times N \times N$ (whose voxels/corners we will denote by $V(\mathcal{G}^N)/K(\mathcal{G}^N)$). †

**Definition 1** Denote by $\mathcal{B}^N$ the space of continuous functions in $\mathbb{R}^3$, with $f \in \mathcal{B}^N$ if and only if for each voxel $v \in V(\mathcal{G}^N)$ there exists a trilinear function $f_v : \mathbb{R}^3 \to \mathbb{R}$ s.t. $f(p) = f_v(p)\ \forall p \in v$.

**Property 1** (Nesting) $\mathcal{B}^N \subset \mathcal{B}^{2N}$

*Proof* When $f \in \mathcal{B}^N$, $\forall v \in V(\mathcal{G}^N)\ \exists\ f_v : \mathbb{R}^3 \to \mathbb{R}$ that is trilinear and $f(p) = f_v(p)\ \forall p \in v$. Since $\forall v' \in V(\mathcal{G}^{2N})\ \exists\ v \in V(\mathcal{G}^N)$ s.t. $v' \subset v$, it follows that $f(p) = f_v(p)\ \forall p \in v'$, and hence $f \in \mathcal{B}^{2N}$. □

Next, the function space $\mathcal{B}^N_{\mathcal{M}}$ on $\mathcal{M}$ is obtained by embedding $\mathcal{M}$ within the voxel grid and considering the restriction of functions in $\mathcal{B}^N$ to $\mathcal{M}$.

**Definition 2** Denote by $\mathcal{B}^N_{\mathcal{M}}$ the space of continuous functions on $\mathcal{M}$, with $f \in \mathcal{B}^N_{\mathcal{M}}$ if and only if for each voxel $v \in V(\mathcal{G}^N)$ there exists a trilinear function $f_v : \mathbb{R}^3 \to \mathbb{R}$ s.t. $f(p) = f_v(p)\ \forall p \in v \cap \mathcal{M}$.

**Property 2** (Nesting) $\mathcal{B}^N_{\mathcal{M}} \subset \mathcal{B}^{2N}_{\mathcal{M}}$

*Proof* When $f \in \mathcal{B}^N_{\mathcal{M}}$, $\forall v \in V(\mathcal{G}^N)\ \exists\ f_v : \mathbb{R}^3 \to \mathbb{R}$ that is trilinear and $f(p) = f_v(p)\ \forall p \in v \cap \mathcal{M}$. Since $\forall v' \in V(\mathcal{G}^{2N})\ \exists\ v \in V(\mathcal{G}^N)$ s.t. $v' \subset v$, it follows that $f(p) = f_v(p)\ \forall p \in v' \cap \mathcal{M}$, and hence $f \in \mathcal{B}^{2N}_{\mathcal{M}}$. □

Using the nesting structure, Chuang *et al.* implement a multigrid solver. Specifically, they use the trilinear B-splines $\{b_k\}$ centered at grid corners $k \in K(\mathcal{G}^N)$ as test functions, and then define the prolongation operator by

$$b_k(p) = \sum_{k' \in K(\mathcal{G}^{2N})} \mathcal{P}^{2N}_N(k,k') \cdot b_{k'}(p) \tag{3}$$

† Though in this work we focus on the piecewise trilinear space of functions, higher order spaces can also be set up, as with [CLB*09].

where $\mathcal{P}^{2N}_N$ is the standard prolongation stencil for 3D B-spline refinement obtained by taking the tensor-product of 1D prolongation stencils: $\frac{1}{4}(1331)$.

## 4. Approach

A limitation of Chuang *et al.*'s approach is that the notion of continuity is characterized with respect to the Euclidean distance rather than the geodesic one. One manifestation of this is that two points adjacent in 3D will necessarily have similar function values, *even if they are geodesically distant*. The inset shows a 2D example, where each of the four B-splines supported on the cell has similar values on $p$ and $q$. As a result, the values of any function in $\mathcal{B}^N_{\mathcal{M}}$ will be *coupled* at $p$ and $q$.

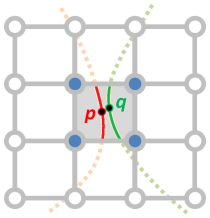


### 4.1. A New Function Space

The goal of this work is to address the coupling problem by enriching $\mathcal{B}^N_{\mathcal{M}}$. In particular, if there exist multiple connected components within a voxel, we will consider assigning a separate basis function to each of them.

**Definition 3** We define $\widetilde{\mathcal{B}}^N_{\mathcal{M}}$ as the space of continuous functions on $\mathcal{M}$ with $f \in \widetilde{\mathcal{B}}^N_{\mathcal{M}}$ if and only if for each voxel $v \in V(\mathcal{G}^N)$ and *each connected component* $c \subset v \cap \mathcal{M}$, there exists a trilinear function $f_c : \mathbb{R}^3 \to \mathbb{R}$ s.t. $f(p) = f_c(p)\ \forall p \in c$.

**Observation** If $c'$ is a connected component of $v' \cap \mathcal{M}$ for some voxel $v' \in V(\mathcal{G}^{2N})$ and $c$ is a connected component of $v \cap \mathcal{M}$ for some voxel $v \in V(\mathcal{G}^N)$, then either $c' \cap c = \emptyset$ or $c' \subset c$. Additionally, for each $c' \subset v' \in V(\mathcal{G}^{2N})$, there must exist a $c \subset v \in V(\mathcal{G}^N)$ s.t. $v' \subset v$ and $c' \subset c$.

**Claim** (Nesting) $\widetilde{\mathcal{B}}^N_{\mathcal{M}} \subset \widetilde{\mathcal{B}}^{2N}_{\mathcal{M}}$

*Proof* When $f \in \widetilde{\mathcal{B}}^N_{\mathcal{M}}$, $\forall v \in V(\mathcal{G}^N)$ and each connected component $c \subset v \cap \mathcal{M}$, $\exists\ f_c : \mathbb{R}^3 \to \mathbb{R}$ that is trilinear and $f(p) = f_c(p)\ \forall p \in c$. Since $\forall v' \in V(\mathcal{G}^{2N})$ and each connected component $c' \subset v' \cap \mathcal{M}$, $\exists c \subset v \cap \mathcal{M}$ for some $v \in V(\mathcal{G}^N)$ s.t. $c' \subset c$, it follows that $f(p) = f_c(p)\ \forall p \in c'$, and hence $f \in \widetilde{\mathcal{B}}^{2N}_{\mathcal{M}}$. □

Note that, as with the work of Chuang *et al.*, the nesting structure of $\widetilde{\mathcal{B}}^N_{\mathcal{M}}$ supports the definition of a multigrid solver.

The advantage of this formulation is highlighted in Figure 1, where the texture on the self-intersecting mesh on the left is projected onto $\mathcal{B}^N_{\mathcal{M}}$ and $\widetilde{\mathcal{B}}^N_{\mathcal{M}}$. In this example, there does not exist a continuous 3D function whose restriction to the mesh can closely represent the texture.

### 4.2. Implementation: Finding The Basis

Chuang *et al.* use first-order, tensor-product B-splines positioned at corners of a regular grid and then discard those

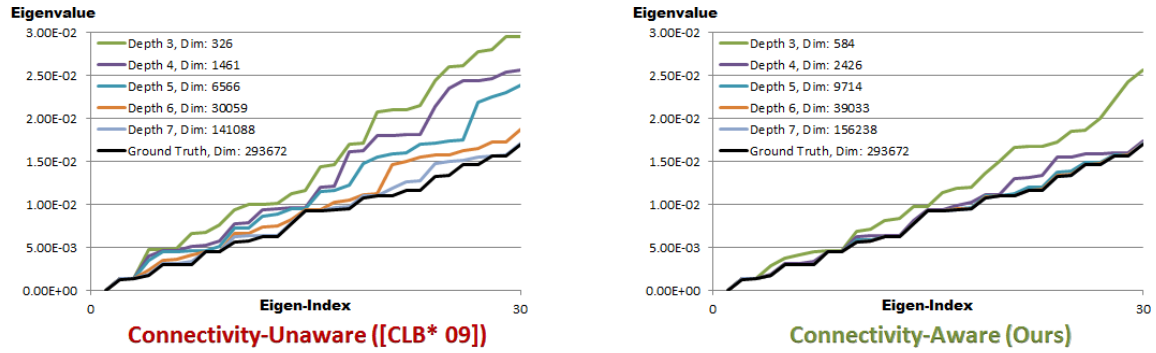


**Figure 3:** *Stability of the spectrum of the estimated Laplace-Beltrami operator. We compute the spectra of Chuang* et al.*'s operator* (left) *and our operator* (right) *at various grid resolutions for the Pulley model* (Figure 4, bottom left). *As the resolution increases, our spectra more quickly converge to the ground-truth.*

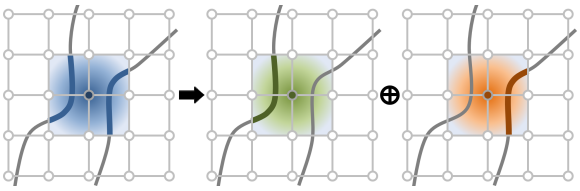

**Figure 2:** *Adaptive splitting of test functions. In [CLB*09], the test functions are chosen independent of the mesh, resulting in disconnected components in the support* (left). *In contrast, our approach refers to mesh connectivity and assigns a separate test function to each component* (middle and right).

test functions whose support does not overlap the surface, to obtain the test functions spanning $\mathcal{B}^N_{\mathcal{M}}$.

In order to obtain our test functions, we start by inspecting the supports of Chuang *et al.*'s functions $\{b_k\}$. At each corner $k \in K(\mathcal{G}^N)$, we generate a separate test function for each connected component of $\mathrm{supp}(b_k) \bigcap \mathcal{M}$ (that is, the intersection of $\mathcal{M}$ with the $2\times 2\times 2$ voxels around $k$). This is illustrated in Figure 2 using a 2D example. We will denote by $I_k$ the number of connected components in the support of $b_k$, and denote by $C^i_k \subset \mathcal{M}$ the $i$-th connected component. Then, each of our test functions $b^i_k$ is duplicated from $b_k$ but is supported only on $C^i_k$:

$$b^i_k(p) = \begin{cases} b_k(p) & \text{if } p \in C^i_k \\ 0 & \text{otherwise.} \end{cases} .$$

### 4.3. Implementation: Multigrid

We obtain our multigrid hierarchy by setting up the test functions (as described in Section 4.2) using grids of successively finer resolutions. As in Chuang *et al.*'s work, every test function $b^i_k$ defined by grid $\mathcal{G}^N$ can be expressed as the linear combination of the test functions $\{b^{i'}_{k'}\}$ defined by grid $\mathcal{G}^{2N}$. Specifically, the prolongation operator is defined by

$$b^i_k(p) = \sum_{k' \in K(\mathcal{G}^{2N})} \sum_{i'=1}^{I_{k'}} \chi\left(C^i_k, C^{i'}_{k'}\right) \cdot \mathcal{P}^{2N}_N(k,k') \cdot b^{i'}_{k'}(p) \quad (4)$$

where

$$\chi(c,c') = \begin{cases} 1 & \text{if } c \cap c' \neq \emptyset \\ 0 & \text{otherwise} \end{cases}$$

indicates if the component $c'$ is contained in $c$.

## 5. Results

In this section, we describe several experiments for evaluating our approach. We start with a spectral analysis that reveals the robustness of our Laplace-Beltrami operator. Next, we examine how the rate of solver convergence is improved by our connectivity-aware space of functions. Finally, we apply our approach to a surface flow application and compare its performance with the state-of-the-art CHOLMOD solver.

### 5.1. Spectral Analysis

Eigendecomposition of the Laplace-Beltrami operator has been widely used for analyzing and processing signal on meshes [Tau95, VL08].

To evaluate the quality of the estimated Laplace-Beltrami operator (Equation 2), Chuang *et al.* compare the spectrum of their operator with the spectrum of the cotangent-weight operator. In particular, this is done by solving the generalized eigenvalue problem:

$$L\mathbf{x} = \lambda M\mathbf{x}$$

with $\mathbf{x}$ a generalized eigenvector and $M$ the mass matrix

$$M_{ij} = \int_{\mathcal{M}} b_i(p) \cdot b_j(p) dp$$

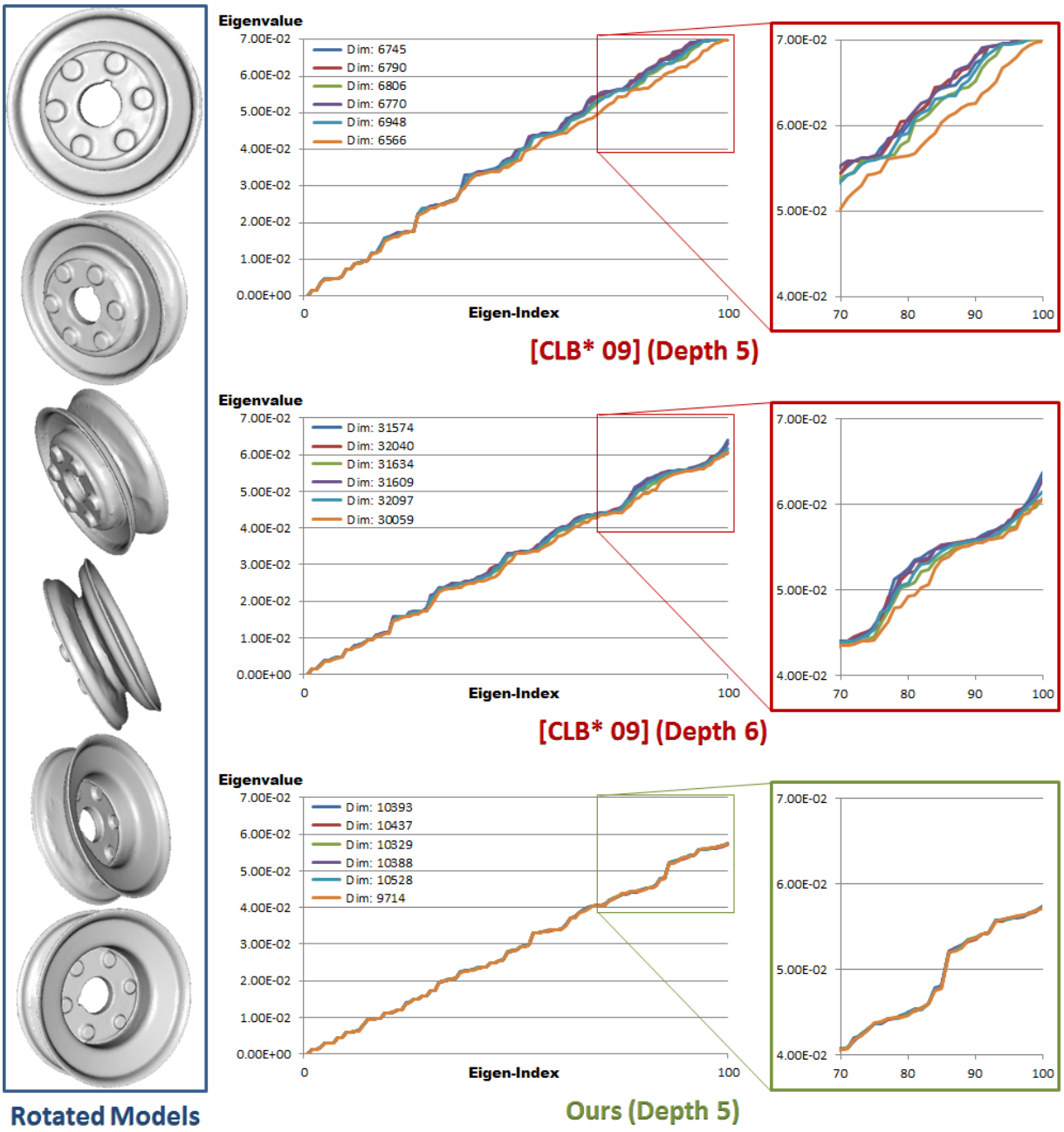


**Figure 4:** *Rotation invariance of the estimated Laplace-Beltrami operator. We compute the spectra of Chuang* et al.*'s operator* (top and middle) *and our operator* (bottom) *for different rotations of the Pulley model. The zoom-ins accentuate the superior stability of our operator* (right).

They show that the idea of restricting regular 3D functions generally helps define a robust Laplace-Belrami opearator whose spectrum is more stable even at a lower dimension (we refer the reader to [CLB*09] for details). However, as they also point out, the approach has difficulty in regions with "narrow cross-sections" – precisely where the coupling of values occurs.

We rerun the experiment on the same model with which

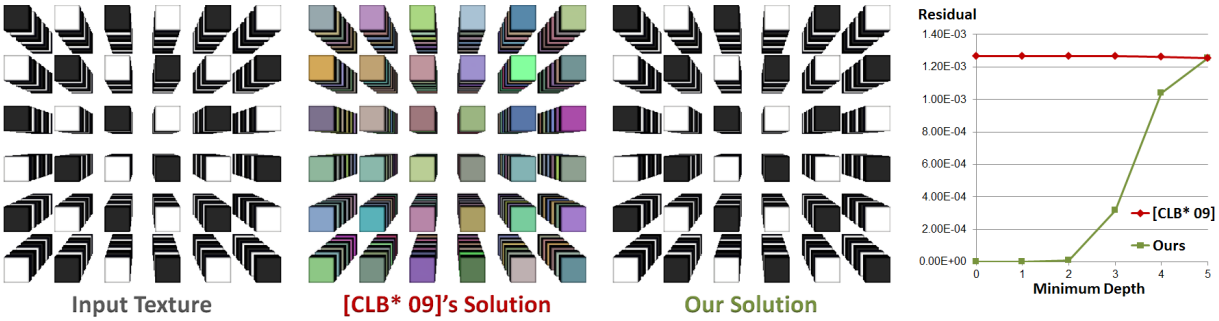


**Figure 5:** *Color fitting of a 3D checker-board texture on the model consisting of equidistantly-spaced* $6 \times 6 \times 6$ *unit-cubes* (left)*. The screened-Poisson equation with the screening weight* $\alpha = 0.01$ *is solved using a grid of depth* 5 *(i.e., consisting of* $2^5 \times 2^5 \times 2^5$ *voxels). The coefficients of the initial guess are generated randomly with values between* 0 *and* 1*. The residuals (normalized by the norm of the initial guess) after one W-cycle are ploted as a function of the minimum depth of the multigrid solver* (right)*, ranging from 0 (i.e., full W-cycle relaxation) to 5 (i.e., Gauss-Seidel relaxation at the finest level only). The texture is reconstructed using Chuang* et al.*'s approach* (middle left) *and our connectivity-aware approach* (middle right).

they had trouble (Figure 4, left). We compute the spectrum at increasing grid resolutions (Figure 3). As demonstrated in the plot, the spectra of our operator quickly converge to the ground truth (computed using the cotangent-weight operator defined over a dense tessellation of the mesh).

We also verify that the rotation-invariance property of the Laplacian is preserved (Figure 4). We apply different rotations to the model before computing the spectrum. Note that even when defining Chuang *et al.*'s operator using a higher resolution grid, our operator still reproduces the spectrum over the different rotations more consistently.

### 5.2. Solver Convergence

As shown in Figure 1, sometimes the connectivity-unaware function space is just not rich enough to express the desired solution. In this section, we examine how the coupling also affects the convergence of the multgrid solver and show that our connectivity-aware approach helps resolve the issue.

In order to make the solver residuals from the different spaces comparable, we use an input model (Figure 5, left) which defines the same function spaces $\mathcal{B}^N_{\mathcal{M}}$ and $\widetilde{\mathcal{B}}^N_{\mathcal{M}}$ at sufficiently fine resolution $N$. This means that the splitting operation of our approach is not necessary at the finest resolution (though it is still necessary at coarser ones). We then solve a screened-Poisson equation on the mesh to reconstruct a color function $f : \mathcal{M} \to \mathbb{R}^3$. That is, given the function $f$, we look for the coefficients $\mathbf{u}$ satisfying:

$$(L + \alpha \cdot M)\mathbf{u} = (\mathbf{f} + \alpha \cdot \mathbf{s})$$

with constraints

$$\mathbf{f}_i = \int_{\mathcal{M}} \langle \nabla f(p), \nabla b_i(p) \rangle dp$$
$$\mathbf{s}_i = \int_{\mathcal{M}} f(p) \cdot b_i(p) dp$$

and screening weight $\alpha = 0.01$. Note that the screening here serves to softly constrain the constant term on each connected component. We perform one standard W-cycle relaxation with ten iterations of Gauss-Seidel smoothing at each level. All coefficeints are intialized with random values between zero and one.

From the results of the reconstruction (Figure 5, middle), we observe that the connectivity-unaware solver does not produce a satisfactory solution, despite the lack of coupling at the finest resolution. We believe this is because the coupling at the coarser spaces prevents multigrid from generating a meaningful correction term.

The plots on the right confirm this. Here we show the magnitude of the residuals as the minimum depth of the multigrid solver is increased. Looking at this plot, we see that increasing the minimum depth does not affect the convergence of the connectivity-unaware solver, indicating that the coarser correction terms do not improve the solution. On the other hand, the convergence of our connectivity-aware solver quickly deteriorates when we increase the minimum depth, suggesting the correct multigrid behavior.

### 5.3. Surface Flow

As pointed out by Chuang *et al.*, although the grid-based approach helps define an effective multigrid, the preprocessing time is significant compared to the solver time. This makes the approach particularly suitable for applications where an

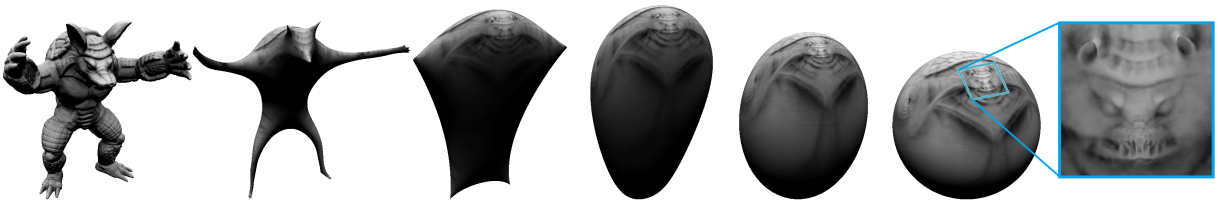

**Figure 6:** *Conformalized Mean-Curvature Flow applied to the Armadillo Man. From left to right, we show the 0th, 1st, 3rd, 5th, 10th and 30th steps of the flow. The flow is numerically stable and conformally evolves the mesh to a sphere* (right).

evolving linear system needs to be solved repeatedly. We evaluate our method in this context.

We apply our approach to support conformalized mean-curvature flow (cMCF) [KSBC12]. The flow, recently proposed by Kazhdan *et al.*, has been shown to converge to a (conformal) spherical parameterization when acting on genus-zero surfaces. Importantly, as opposed to traditional mean-curvature flow, cMCF does not develop singularities and is numerically stable, making it well-suited for studying the long-term behavior of our solver.

At each time $t$, we solve a semi-implicit system as described in [DMSB99]:

$$\left(M_t + \frac{\delta}{2} L_0\right) \mathbf{u}_{t+\delta} = M_t \mathbf{u}_t$$

with $\delta$ the temporal stepsize, $M_t$ the mass matrix of the surface at time $t$, and $L_0$ the stiffness matrix of the original surface. Figure 6 shows an example of the flow.

**Performance** When performing surface flow, it is often necessary to consider the trade-offs between the computational cost and the solution accuracy. Factors affecting the computational cost include the temporal stepsize (as taking smaller timesteps increases the temporal resolution but leads to longer running time) and the solver time per step (as using more accurate solvers increases the accuracy within each timestep but leads to longer running time).

We first simulate the ground truth cMCF on a high resolution brain model consisting of 1.4 millions vertices (Figure 8, left). The evolution time is targeted at $t = 50$ and we take a tiny stepsize $\delta = 0.01$ to flow the surface toward the target. At each time step, we use the cotangent-weight operator to define the system, which is then solved precisely by CHOLMOD. The simulation takes more than 10 hours to generate all the evolved surfaces on a PC with an i7-2820QM processor. Having computed these, we later generate the ground truth at any $t = \tau$ by linearly interpolating the surfaces at $t = \lfloor \frac{\tau}{\delta} \rfloor \delta$ and $t = \lceil \frac{\tau}{\delta} \rceil \delta$.

Next, we run the flow using the following configurations of systems and solvers: ‡

- Cotangent-weight System solved by CHOLMOD
- Chuang *et al.*'s system solved by CHOLMOD
- Chuang *et al.*'s system solved by Multigrid
- Our system solved by CHOLMOD
- Our system solved by Multigrid

For the grid-based systems (all but the first), we follow Chuang *et al.*'s formulation of test function tracking, in order to avoid having to set up the multigrid hierarchy repeatedly as the embedding changes [CK11a]. We choose a grid resolution of $2^8 \times 2^8 \times 2^8$ so that the resulting dimension is roughly the same as that of the cotangent-weight system. §

We require each configuration to complete the flow within one hundred seconds. As the evolution time is fixed at $t = 50$, the temporal stepsize $\delta$ taken by each configuration depends on how quickly each spacial system is solved, as summarized in Table 1.

Finally, we compare the evolved surfaces obtained from each configuration to the ground truth. Results are shown in Figure 7, where we plot the RMS error ($\sqrt{\sum_i \|v_i^e - v_i^g\|^2}$ with $v^e$ and $v^g$ the evovled and ground truth vertex positions) as a function of evolution time. Here we make two observations. First, although the direct solver is capable of computing exact solutions, the expensive cost prevents us from taking small timesteps and eventually leads to larger errors. Second, the connectivity-unaware and connectivity-aware multigrid systems perform equally well in the begining, but then the connectivity-unaware one deteriorates quickly with time. In Figure 8, we examine the two surfaces at the end of the flow. The zoom-ins highlight the problem of the connectivity-unaware approach, where the values of the

‡ Our CHOLMOD is compiled by the Intel Math Kernel Library [MKL12] to ensure the best performance. In addition, the symbolic factorization is only performed once in the preprocessing.

§ When the dimensions match, solving the grid-based systems is more costly than solving the cotangent-weight system, as the grid-based systems are less sparse (the average number of entries per row is 18, compared to 7 for the cotangent-weight Laplacian).

| Configuration (System + Solver) | | Dimension | Non-Zero Entries | Time/Step | Steps | Stepsize (δ) |
|---|---|---|---|---|---|---|
| Cotangent | + CHOLMOD | $1.38 \times 10^6$ | $9.67 \times 10^6$ | 3.78 | 26 | 1.92 |
| [CLB* 09] | + CHOLMOD | $1.21 \times 10^6$ | $2.22 \times 10^7$ | 11.08 | 9 | 5.56 |
| | + Multigrid | | | 1.47 | 68 | 0.74 |
| Ours | + CHOLMOD | $1.27 \times 10^6$ | $2.28 \times 10^7$ | 9.26 | 10 | 5.00 |
| | + Multigrid | | | 1.52 | 66 | 0.76 |

**Table 1:** *Statistics for the different configurations, giving the system dimension, the number of non-zero entries, the average time spent for each time step (including the time for updating the system/solver and the time for solving the system), the total number of steps, and the temporal step size.*

coordinate function are coupled across the two hemispheres of the brain and cannot flow independently.

### Discussion

Using our formulation, we resolve the problem of value coupling across disconnected components. However, we *cannot* decouple function values for points on the *same* component. The problem becomes manifest when the grid resolution is low and the surface has high curvature. In Figure 10, we visualize the support of one basis function of our system defined using a lower resolution grid (depth 7). The support contains two flat regions that meet near a corner. As a result, running cMCF at this low resolution results in pronounced errors in these regions.

Another issue with grid-based systems, is the possible presence of *linear dependency*. That is, when there exists an entirely planar component aligned with one of the axes (i.e. not in *general position*), the linear system becomes singular. In pratice this is not a problem, because our multigrid solver uses a Gauss-Seidel smoother, which is guaranteed to converge for symmetric and positive definite systems and tends to behave well even when the system is only positive semi-definite. This can become a problem when using a direct solver like CHOLMOD. However, this issue can be resolved, either by applying a slight rotation to the model, or by adding a diagonal term, $\varepsilon \cdot \mathbf{Id}$, with $\varepsilon$ a small constant, to the system.

Finally, one can interpret our connectivity-aware adaptation of the FEM construction as a refinement of a point-set topology on the surface. Specifically, if one defines a simple topology on $\mathbb{R}$ consisting of the open sets $X(\mathbb{R}) = \{\emptyset, \mathbb{R} - \{0\}, \mathbb{R}\}$, then any choice of basis functions $\{b_1, \ldots, b_N\}$ defines a topology $X(\mathcal{M})$ on the mesh, generated by the unions and intersections of the sets $b_i^{-1}(U)$, with $U \in X(\mathbb{R})$. By splitting basis functions based on connectivity, we obtain a finer set set of generators for a topology on $\mathcal{M}$, reflecting the better localization of the connectivity-aware function space.

## 6. Conclusion

In this work, we present an important extension to grid-based systems for solving Poisson equations on surfaces. Our formulation addresses the coupling issue arising in earlier work by incorporating local connectivity information in defining an FEM discretization. The resulting function space has several advantages: It defines a robust Laplace-Beltrami operator (5.1). It improves the multigrid behavior (5.2). And, it provides an effective system for performing surface evolution (5.3).

In the future, we would like to explore extension of our approach to feature-adaptive refinement of test functions (in particular, near the high-curvature regions where the coupling problem still occurs). We would also like to apply our approach to support other applications that can benefit from a real-time iterative solver, such as cloth simulation and more general surface flows.

## References

[AKS05] AKSOYLU B., KHODAKOVSKY A., SCHRÖDER P.: Multilevel solvers for unstructured surface meshes. *SIAM Journal of Scientific Computing 26* (2005), 1146–1165. 2

[BCF*01] BREZINA M., CLEARY J., FALGOUT R., HENSON V., JONES J., MANTEUFFEL T., MCCORMICK S., RUGE J.: Algebraic multigrid based on element interpolation (AMGe). *SIAM Journal of Scientific Computing 22*, 5 (2001), 1570–1592. 2

[BHM00] BRIGGS W., HENSON V., MCCORMICK S.: *A Multigrid Tutorial*. Society for Industrial and Applied Mathematics, 2000. 2

[BS07] BOBENKO A. I., SPRINGBORN B. A.: A discrete Laplace-Beltrami operator for simplicial surfaces. *Discrete Comput. Geom. 38*, 4 (Dec. 2007), 740–756. 2

[CDR00] CLARENZ U., DIEWALD U., RUMPF M.: Anisotropic geometric diffusion in surface processing. In *Visualization '00: Proceedings of the 11th IEEE Visualization 2000 Conference (VIS 2000)* (2000), pp. 497–405. 2

[CFH*00] CLEARY A. J., FALGOUT R. D., HENSON V. E., JONES J. E., MANTEUFFEL T. A., MCCORMICK S. F., MIRANDA G. N., RUGE J. W.: Robustness and scalability of algebraic multigrid. *SIAM Journal of Scientific Computing 21*, 5 (2000), 1886–1908. 2

[CFH*03] CHARTIER T., FALGOUT R. D., HENSON V. E.,

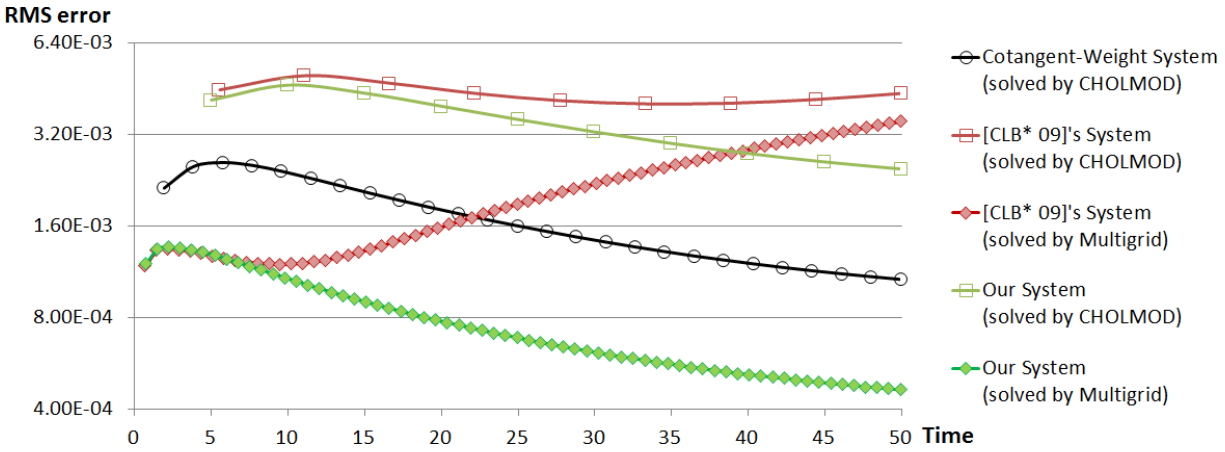


**Figure 7:** *Error comparison of the different approaches performing* cMCF *on a brain model consisting of 1.4 million vertices. The RMS error is plotted as a function of evolution time. The ground truth is simulated using* CHOLMOD *to solve the cotangent-weight system taking a tiny stepsize* $\delta = 0.01$. *The computational budget is fixed at one hundred seconds , so that the number of steps (visualized by the tick marks) is determined by the efficiency of the solver.*

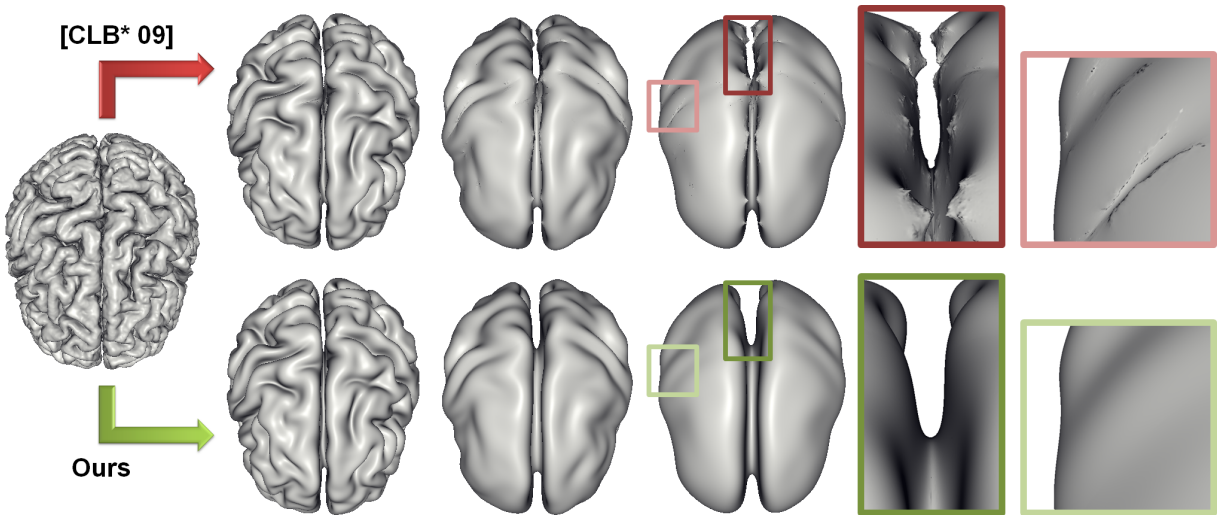


**Figure 8:** *The brain undergoing* cMCF *with the connectivity-unaware* ([CLB* 09]) *and connectivity-aware* (ours) *function spaces used to define the system for the input mesh* (left). *The two systems have about the same dimension and are both solved using the multigrid. Here we show the evovled surfaces at* $t = 10$, $t = 25$, *and* $t = 50$ (middle). *The zoom-ins highlight the benefit of using the connectivity-aware system, which is able to decouple the function values at points that are close in Euclidean space, allowing them to flow independently* (right).

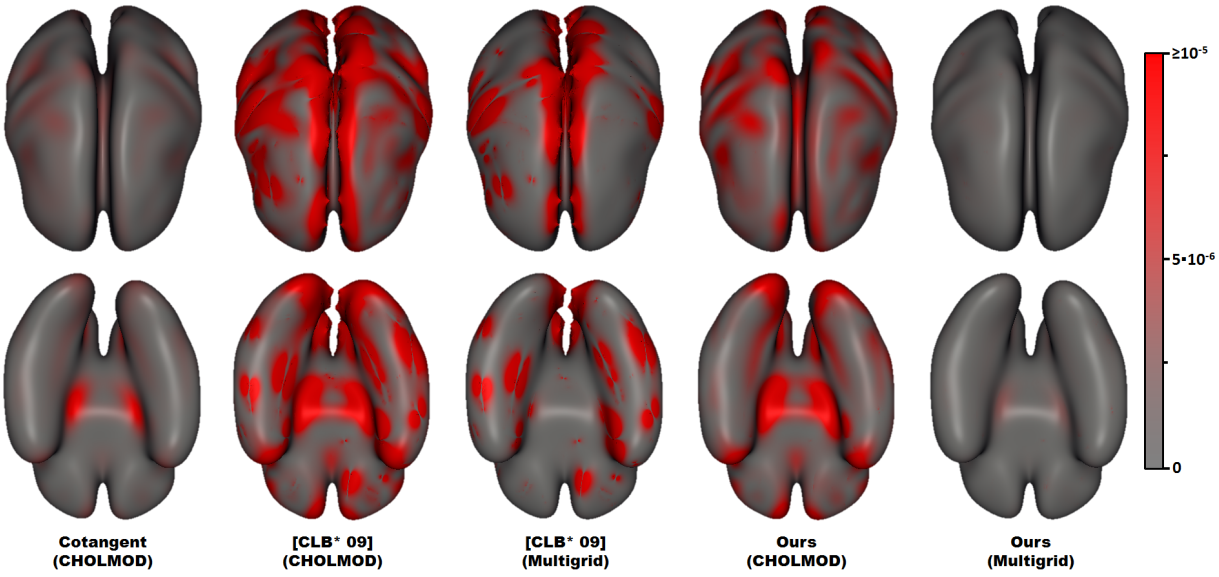


**Figure 9:** *Error visualization of the* cMCF *evolution by the different configurations at time* $t = 50$*. We draw on the mesh the per-vertex squared distance to the ground truth in red. Note that for the connectivity-unaware systems, errors accumulate quickly around those "pinched" regions.*

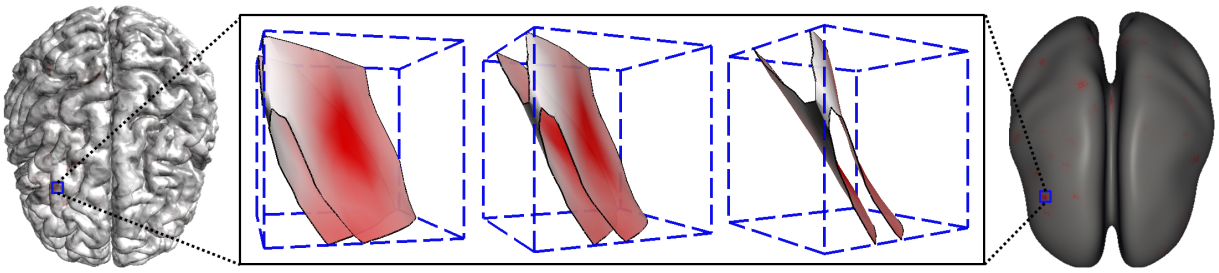

**Figure 10:** *Value coupling within a connected component near a high curvature region of the brain* (left)*. When we define our system using a lower resolution grid, there exists a basis function supported on two parallel patches. Rendering the support from different perspectives, we observe that the function cannot be split because the two partches are connected at the corner* (middle)*. As a result, performing* cMCF *using this lower resolution system yields high errors on the evolved surface* (left, drawn as in Figure 9).

JONES J., MANTEUFFEL T., MCCORMICK S., RUGE J., VASSILEVSKI P. S.: Spectral AMGe (ρAMGe). *SIAM Journal of Scientific Computing 25*, 1 (2003), 1–26. 2

[CK11a] CHUANG M., KAZHDAN M.: Fast mean-curvature flow via finite-elements tracking. *Computer Graphics Forum 30*, 6 (2011), 1750–1760. 2, 7

[CK11b] CHUANG M., KAZHDAN M.: Interactive and anisotropic geometry processing using the screened poisson equation. *ACM Transactions on Graphics (SIGGRAPH '11)* (2011). 2

[CLB*09] CHUANG M., LUO L., BROWN B., RUSINKIEWICZ S., KAZHDAN M.: Estimating the Laplace-Beltrami operator by restricting 3D functions. *Computer Graphics Forum (Symposium on Geometry Processing)* (2009), 1475–1484. 2, 3, 4, 5

[Dav04] DAVIS T. A.: Algorithm 832: UMFPACK V4.3—an unsymmetric-pattern multifrontal method. *ACM Transactions On Mathematical Software 30*, 2 (2004), 196–199. 2

[Dav11] DAVIS T. A.: User guide for CHOLMOD: a sparse cholesky factorization and modification package. http://www.cise.ufl.edu/research/sparse/cholmod/CHOLMOD/Doc/UserGuide.pdf, 2011. 2

[DH99] DAVIS T. A., HAGER W. W.: Modifying a sparse cholesky factorization. *SIAM Journal on Matrix Analysis and Applications 20*, 3 (1999), 606–627. 2

[DMSB99] DESBRUN M., MEYER M., SCHRÖDER P., BARR A.: Implicit fairing of irregular meshes using diffusion and

curvature flow. In *ACM SIGGRAPH Conference Proceedings* (1999), pp. 317–324. 2, 7

[Dzi88] DZIUK G.: Finite elements for the Beltrami operator on arbitrary surfaces. In *Partial Differential Equations and Calculus of Variations*, vol. 1357 of *Lecture Notes in Mathematics*. Springer Berlin / Heidelberg, 1988, pp. 142–155. 2

[FH05] FLOATER M. S., HORMANN K.: Surface parameterization: a tutorial and survey. In *In Advances in Multiresolution for Geometric Modelling* (2005), Springer, pp. 157–186. 2

[Flo03] FLOATER M. S.: Mean value coordinates. *Computer Aided Geometric Design 20* (2003), 2003. 2

[FSBS06] FISHER M., SPRINGBORN B., BOBENKO A. I., SCHRODER P.: An algorithm for the construction of intrinsic delaunay triangulations with applications to digital geometry processing. In *ACM SIGGRAPH 2006 Courses* (2006), SIGGRAPH '06, pp. 69–74. 2

[GVL96] GOLUB G. H., VAN LOAN C. F.: *Matrix computations (3rd ed.)*. Johns Hopkins University Press, Baltimore, MD, USA, 1996. 2

[HY00] HENSON V. E., YANG U. M.: Boomeramg: A parallel algebraic multigrid solver and preconditioner. *Applied Numerical Mathematics 41* (2000), 155–177. 2

[KBH06] KAZHDAN M., BOLITHO M., HOPPE H.: Poisson surface reconstruction. In *Proceedings of the fourth Eurographics Symposium on Geometry processing* (Aire-la-Ville, Switzerland, Switzerland, 2006), SGP '06, Eurographics Association, pp. 61–70. 2

[KCVS98] KOBBELT L., CAMPAGNA S., VORSATZ J., SEIDEL H.: Interactive multi-resolution modeling on arbitrary meshes. In *SIGGRAPH '98: Proceedings of the 25th annual conference on Computer graphics and interactive techniques* (1998), pp. 105–114. 2

[KSBC12] KAZHDAN M., SOLOMON J., BEN-CHEN M.: Can Mean-Curvature Flow be Modified to be Non-singular? *Computer Graphics Forum (Symposium on Geometry Processing)* (2012). 7

[Li05] LI X. S.: An overview of SuperLU: Algorithms, implementation, and user interface. *ACM Trans. Math. Softw. 31*, 3 (September 2005), 302–325. 2

[MKL12] MATH KERNEL LIBRARY 10.3 I.: http://software.intel.com/en-us/articles/intel-mkl/, 2012. 7

[PP93] PINKALL U., POLTHIER K.: Computing discrete minimal surfaces and their conjugates. *Experimental Mathematics 2* (1993), 15–36. 2

[RL03] RAY N., LEVY B.: Hierarchical least squares conformal map. In *Pacific Graphics* (2003), p. 263. 2

[RS87] RUGE J., STUEBEN K.: Algebraic multigrid. 73–130. 2

[SA07] SORKINE O., ALEXA M.: As-rigid-as-possible surface modeling. In *Proceedings of EUROGRAPHICS/ACM SIGGRAPH Symposium on Geometry Processing* (2007), pp. 109–116. 2

[SBZ09] SHI X., BAO H., ZHOU K.: Out-of-core multigrid solver for streaming meshes. *ACM Transactions on Graphics (SIGGRAPH Asia '09) 28*, 5 (2009). 2

[SCOL*04] SORKINE O., COHEN-OR D., LIPMAN Y., ROSSL C., SEIDEL H.: Laplacian surface editing. In *Eurographics/ACM SIGGRAPH Symposium on Geometry Processing* (2004), pp. 179–188. 2

[SK01] SCHNEIDER R., KOBBELT L.: Geometric fairing of irregular meshes for free-form surface design. *Computer Aided Geometric Design 18* (2001), 359–379. 2

[SYBF06] SHI L., YU Y., BELL N., FENG W.-W.: A fast multigrid algorithm for mesh deformation. *ACM Transactions on Graph (SIGGRAPH '06) 25*, 3 (2006), 1108–1117. 2

[Tau95] TAUBIN G.: A signal processing approach to fair surface design. In *ACM SIGGRAPH* (1995), pp. 351–358. 2, 4

[VL08] VALLET B., LÉVY B.: Spectral geometry processing with manifold harmonics. *Computer Graphics Forum (Proceedings Eurographics)* (2008). 4

[WMKG07] WARDETZKY M., MATHUR S., KÄLBERER F., GRINSPUN E.: Discrete laplace operators: no free lunch. In *Proceedings of the fifth Eurographics symposium on Geometry processing* (2007), SGP '07, Eurographics Association, pp. 33–37. 2

[Zha04] ZHANG H.: Discrete combinatorial laplacian operators for digital geometry processing. In *SIAM Conference on Geometric Design, 2004* (2004), Press, pp. 575–592. 2